Supplementary Information

Dipole-field interaction: a missing link to bridge the gap between theoretical and experimental catalysis in single-atom electrocatalyst for CO_2 reduction

Ruirui Ren,[a] Yuhang Wang, [a,b*] Bo Li, [a,*] Jun Fan [b,*]

[a]*College of Chemistry and Pharmaceutical Engineering, Nanyang Normal University, Nanyang 473061, PR China*

[b]*Department of Materials Science and Engineering, City University of Hong Kong, Hong Kong, 999077, China.*

[*] Corresponding author

Supplementary Information

1. Computational methods

1.1 Density functional theory calculation method

All periodic DFT calculations in this work were performed with the VASP package[1]. The ion–electron interactions were described by the projector augmented wave (PAW) method, and the valence wavefunctions were expanded using a plane-wave basis set with a cutoff energy of 400 eV. For the exchange–correlation functional, the revised Perdew–Burke–Ernzerhof (RPBE) functional within the generalized gradient approximation (GGA) was adopted[1, 2]. This functional was chosen based on previous benchmark studies that compared theoretical predictions with experimental results[3, 4]. Structural optimizations were carried out until the residual forces on each atom fell below 0.05 eV Å^{-1}, and the total energy was converged to within 10^{-5} eV. The Brillouin zone was sampled using a Γ-centered Monkhorst–Pack mesh, where the k-point spacing was automatically generated to be less than 0.4 Å^{-1}. A vacuum layer of 15 Å was introduced along the direction perpendicular to the surface to eliminate spurious interactions between neighbouring slabs. A schematic illustration of the model construction is shown in **Figure S1**. The pristine graphene-based structure has dimensions of 8.56 Å × 9.87 Å. By substituting two carbon atoms with metal atoms (indicated by the red dashed circle/line), Fe/Co/Ni-based single-atom catalysts with different non-metal coordination environments are constructed.

1.2 Free energy calculation of CO_2 electroreduction

The adsorption energy of reaction intermediates ($\Delta E(^{*}C_xH_yO_z)$) during CO_2 reduction reaction (CO_2RR) was calculated as:

$$\Delta E(^{*}C_xH_yO_z) = E(*C_xH_yO_z) - E(^{*}) - x \cdot E(C) - y \cdot E(H) - z \cdot E(O), \quad (1)$$

where $E(^{*}C_xH_yO_z)$ and $E(^{*})$ mean the free energy of $C_xH_yO_z$ species adsorbed on the surface and slab surface $(^{*})$, respectively. The calculation of $E(C)$, $E(H)$, and $E(O)$ are based on the energies of CO_2, H_2, respectively. The free energy of each elementary step for CO_2RR was defined by employing previous methods by Nørskov and his collaborators[5]:

$$\Delta G = \Delta E + \Delta E_{ZPE} + \int C_p dT - T \cdot \Delta S + E_{solv}, \quad (2)$$

where ΔE means the difference in DFT electronic energy, ΔE_{ZPE}, $\int C_p dT$ and ΔS refer to the zero point energy, heat capacities, and entropy corrections, and T is the absolute temperature, set to 298.15 K. The zero point energy and entropic contribution $(T \cdot \Delta S)$ were obtained with the harmonic approximation. E_{solv} is the solvation corrections described in Ref.[6]. To improve the energetics of gas-phase species, energy correction for CO_2 (0.29 eV) and H_2 (0.09 eV) are considered for accounting the systematic DFT errors in catalytic reactions[7].

1.3 Charge density difference calculation

The charge density differences (Δρ) were calculated using the following equation:

$$\Delta\rho = \rho_{\text{tot}} - \rho_{\text{bare}} - \rho_{Adsorbate}, \quad (3)$$

where ρ_{tot} is the charge density of the surface with the adsorbed molecules, ρ_{bare} is the charge density of the bare surface, and $\rho_{Adsorbate}$ is the charge density of the adsorbate.

1.4 Electric fields and pH-dependent modelling at the RHE-scale

An external electric field was simulated by introducing a saw-tooth electrostatic potential along the direction perpendicular to the surface. For each field strength applied, the adsorption configurations were fully optimized until the residual forces on all atoms were below 0.05 eV/Å, and the most stable structure was then used to determine the corresponding adsorbate energy. The choice of this range is justified by two considerations: (1) it adequately covers the field variations relevant to the applied potentials and pH conditions in CO_2RR, as widely adopted in the field[8, 9]; (2) the symmetric range centered at zero enables reliable extraction of dipole moments and polarizabilities via quadratic fitting, a standard approach in electrocatalysis[10, 11]. To establish a direct connection between the computed electric fields and experimentally relevant conditions, a parallel-plate capacitor model was employed to correlate the field strength with both the standard hydrogen electrode (SHE) and reversible hydrogen electrode (RHE) scales. The model is described by equation 10, where σ refers to charge density, ε_0 refers to the vacuum permittivity (8.85×10^{-12} F m^{-1}), ε refers to the dielectric constant (unitless), C_H refers to

the Helmholtz capacitance (μF cm^{-2}), U_{SHE} refers to the potential *vs*. SHE, and U_{PZC} refers to the potential at the point of zero charges *vs*. SHE.

$$\vec{E} = \frac{\sigma}{\varepsilon\varepsilon_0} = \frac{C_H(U_{SHE} - U_{PZC})}{\varepsilon\varepsilon_0}, \quad (4)$$

Fumagalli et al.[12] demonstrated that the dielectric constant of water near a surface is 2. The Helmholtz capacitance (C_H) can vary with the surface and potential and determined based on the description shown in Ref. [13].

As described by equation 10, the electric field depends on the absolute potential of an electrode. It can be measured by using a standard hydrogen electrode (U_{SHE}), which relates to RHE (reversible hydrogen electrode) by equation 5.

$$U_{SHE} = U_{RHE} - k_b T ln(10) \times pH = U_{RHE} - 0.059\, pH, \quad (5)$$

Field-dependent energy corrections are considered using a second-order polynomial form shown in equation 12:

$$G_{ads} = G_{ads}^{PZC} + \mu\vec{E} - \frac{\alpha}{2}\vec{E}^2, \quad (6)$$

G_{ads}^{PZC} denotes the binding energy of adsorbate at the potential of zero charge, representing the energy computed without an applied field. The intrinsic dipole moment (μ) and polarizability (α) can be determined by fitting the G_{ads} and applied field $\vec{E}$.

Then, effect of electrode potential on intermediates adsorption energy can be estimated by the following mathematical expression:

$$G_{ads} = G_{ads}^{PZC} + \mu\frac{C_H(U_{SHE} - U_{PZC})}{\varepsilon\varepsilon_0} - \frac{\alpha}{2}\left(\frac{C_H(U_{SHE} - U_{PZC})}{\varepsilon\varepsilon_0}\right)^2, \quad (7)$$

$$G_{ads} = G_{ads}^{PZC} + \mu\frac{C_H(U_{RHE} - 0.059pH - U_{PZC})}{\varepsilon\varepsilon_0} - \frac{\alpha}{2}\left(\frac{C_H(U_{RHE} - 0.059pH - U_{PZC})}{\varepsilon\varepsilon_0}\right)^2, \quad (8)$$

1.5 Calculation of the Potential of Zero Charge

AIMD simulations of metal-water interfaces have emerged as the more accurate method to estimate PZCs[14-17].AIMD simulations were performed with VASP using the RPBE exchange-correlation functional[1, 2], and included the D3 dispersion correction scheme[18], recognized for its precision in describing metal−water interfaces[19, 20]. A plane-wave cutoff energy of 400 eV was utilized in our simulations. The electronic structure was optimized until all forces were below 0.05 eV/Å. *Γ*-point AIMD simulations were performed with a 1 fs time step, and a Nosé thermostat was maintained at 300 K. The metal−water interfaces for single atom catalysts comprised a water layer of at least 10 Å in height, corresponding to a water density of 1 g/cm^3. Trasatti *et al.*[21] showed that U_{PZC} could be directly derived from the work function of a material in ion-free water ϕ using equation 9:

$$\phi = eU_{PZC} + e\phi_{SHE}, \quad (9)$$

Here, ϕ_{SHE} represents the absolute potential energy of the SHE. It is important to note that the value of ϕ_{SHE} can vary depending on the experiment conducted (ranging from 4.3 to 4.8 eV). However, in this study, the recommended value of 4.44 eV by the International Union of Pure and Applied Chemistry (IUPAC) was used.

1.6 Microkinetic modelling

The microkinetic modelling of the CO_2RR volcano was based on the approach outlined by Hansen *et al.* [22] and Kelly *et al.*[13]. Rates for intermediate steps were calculated as below:

$$rate = k_f \prod \theta_{reac} - k_b \prod \theta_{prod}, \quad (10)$$

where θ_{reac} and θ_{prod} are the coverages of reactants and products, respectively. k_f and k_b are the rate constant of forwards and backwards reaction, which were calculated as the function of reaction perfector A (s^{-1}), activation free energy G_a, Boltzmann constant k_B, and reaction temperature T:

$$k = Ae^{-\frac{G_a}{k_B T}}, \quad (11)$$

The intermediate for CO formation considered in the modelling are shown in Reactions (12-14):

$$CO_2(g) + * + H^+ + e^- \rightarrow *COOH, \quad (12)$$

$$*COOH + H^+ + e^- \rightarrow *CO + H_2O, \quad (13)$$

$$*CO \rightarrow CO + *, \quad (14)$$

Reactions (12-14) involve proton-electron transfer steps, where the energy of the proton-electron pair is represented by the energy of half of a H_2 molecule according to the CHE method[5]. Besides, we incorporate an intrinsic barrier of 0.26 eV to the free-energy diagram to correlate the thermodynamic to the kinetic, which is commonly used in electrocatalysis studies to account for the proton-electron transfer step[10, 22, 23].

2. Supplementary tables and figures

Figure S1

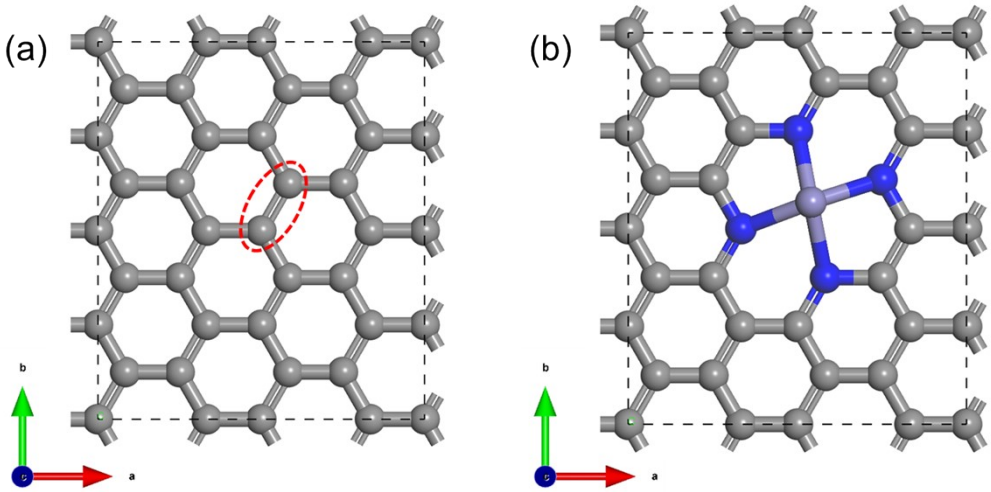

Fig. S1 Schematic illustration of model construction, taking the Fe–N_4 structure as an example. (a) Top view of the pristine graphene structure; (b) top view of the Fe–N_4-based single-atom structure. Color code: gray for C; blue for N; light purple for Fe.

Figure S2

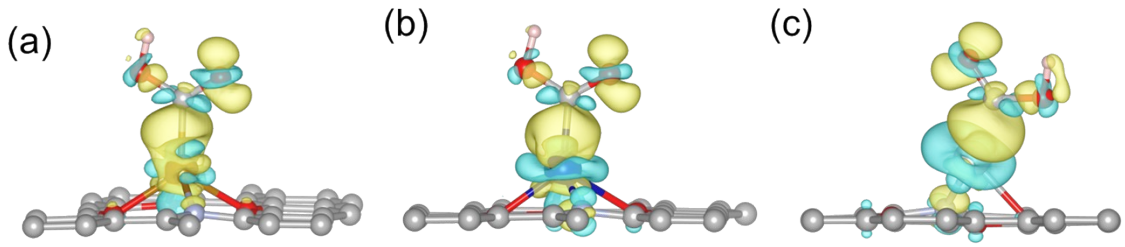

Fig. S2 Charge density difference plots induced by the adsorption of *COOH. Yellow and teal isosurfaces represent electron accumulation and depletion, respectively. Atom color scheme: brown (Fe), blue (Co), light blue (Ni), gray (C), red (O), silver (N), and light pink (H).

Figure S3

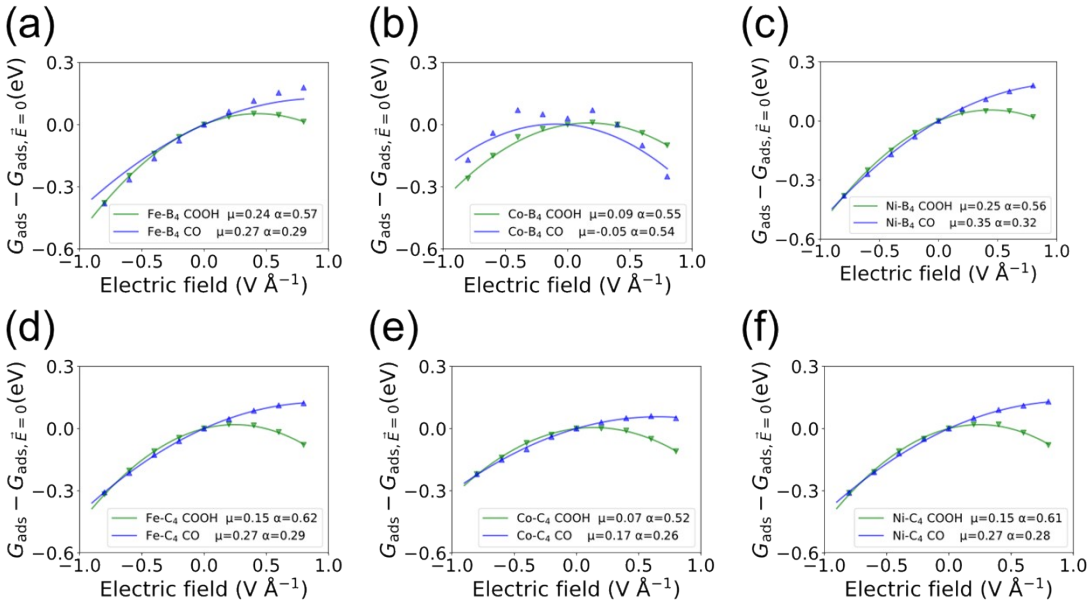

Fig. S3 Electric-field effects on the adsorption free energies of key CO_2RR intermediates on M–X_4 sites (M = Fe, Co, Ni, X=B,C).

Figure S4

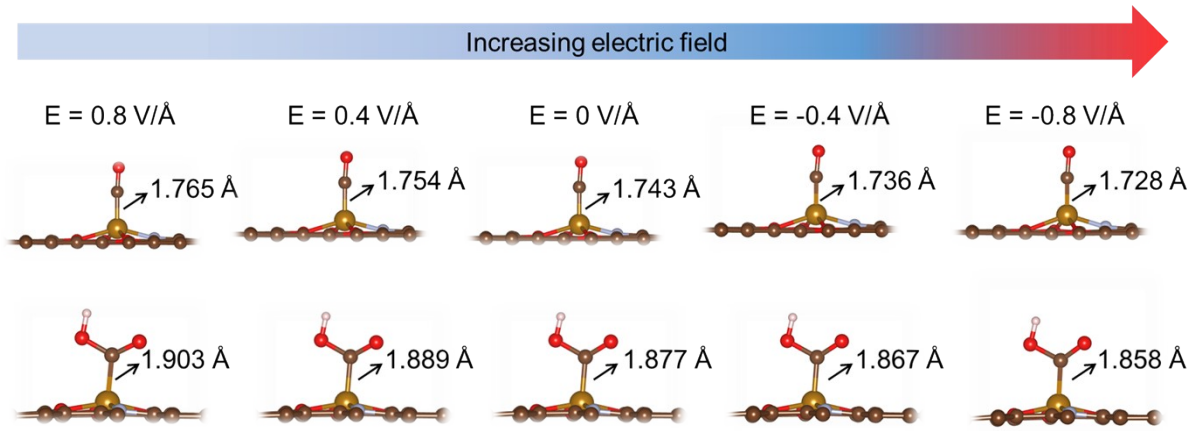

Fig. S4 Electric-field-dependent variation of the Fe–C bond length for *CO and *COOH adsorbed on the Fe–O_3N surface. Atom colors: Fe (brown), C (dark brown), O (red), H (light pink), and N (gray).

Figure S5

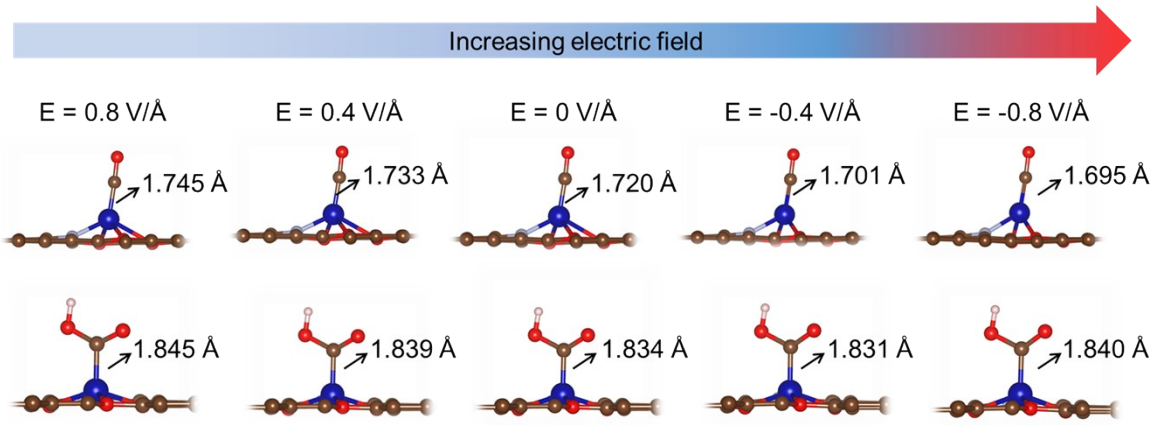

Fig. S5 Electric-field-dependent variation of the Co–C bond length for *CO and *COOH adsorbed on the Co–O_3N surface. Atom colors: Co (blue), C (brown), O (red), H (light pink), and N (gray).

Figure S6

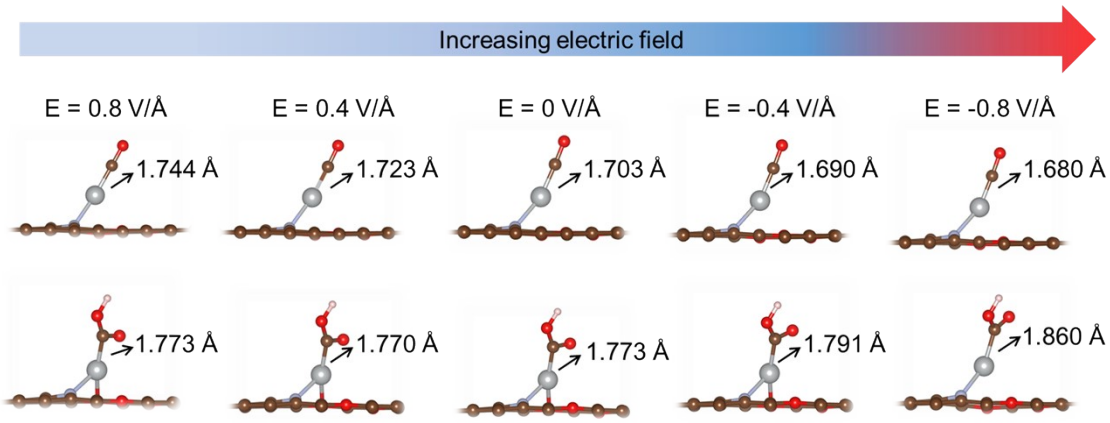

Fig. S6 Electric-field-dependent variation of the Ni–C bond length for *CO and *COOH adsorbed on the Ni–O_3N surface. Atom colors: Ni (silver), C (dark brown), O (red), H (light pink), and N (gray).

Figure S7

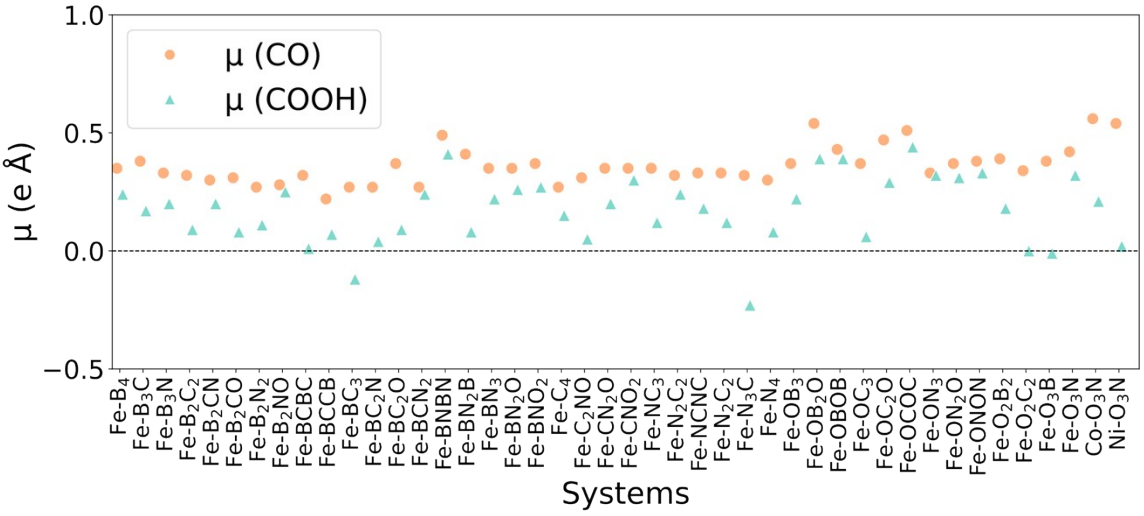

Fig. S7 Comparison of dipole moments of *CO and *COOH on different catalyst surfaces.

Figure S8

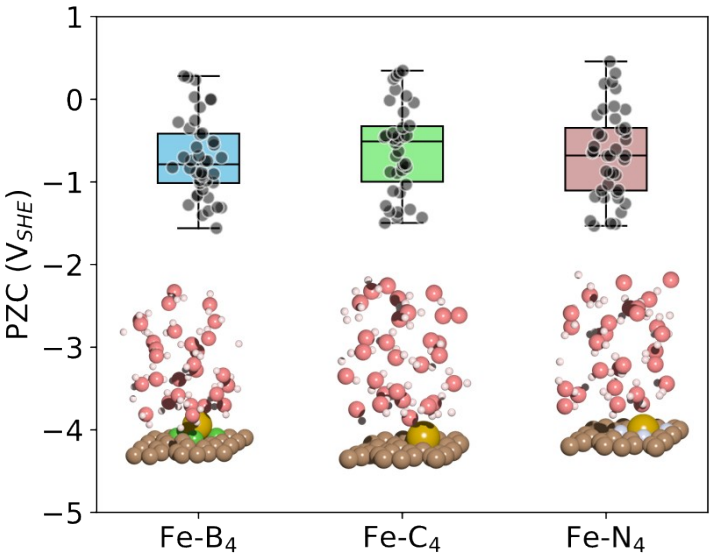

Fig. S8 Potential of zero-charges (PZCs) calculated from explicit solvation models based on AIMD simulations. The structures were sampled from at least 30 distinct surface–adsorbate configurations, followed by DFT optimization after 5000 fs of AIMD simulations. Insets illustrate the explicit solvation models of Fe–X_4 (X = B, C, N). Atom colors: Fe (light brown), B (green), C (dark brown), N (gray), O (red), and H (light pink).

Figure S9

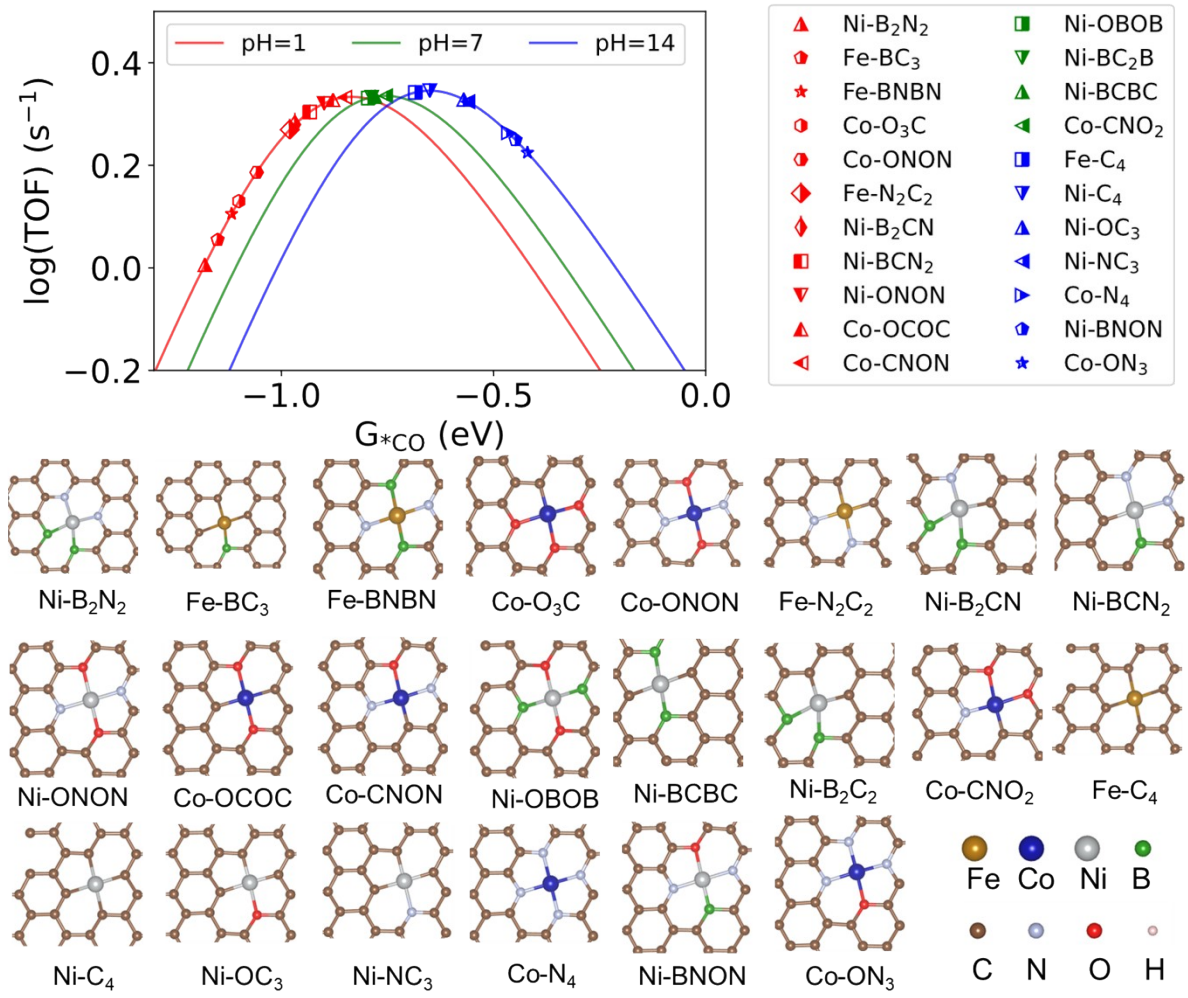

Fig S9. Prediction on new M-N-C catalysts toward CO formation. pH-dependent volcano models for HCOOH production obtained from theoretical predictions at -1.0 V_{RHE} under various pH ranges. The binding free energies were calculated with solvation corrections. The energies used for the calculation of adsorption free energy is listed in **Table S2**.

Table S1

Table S1 Summary of dipole moments and polarizabilities of *CO and *COOH adsorbed on single-atom catalysts with different coordination environments. Because Fe-, Co-, and Ni-based single-atom catalysts exhibit similar dipole–field interactions for *CO and *COOH adsorption, we focused on all Fe coordination environments and representative Co and Ni configurations to reduce computational cost. The averaged properties of all catalyst surfaces were subsequently used for the derivation of the volcano plots.

Systems	*CO		*COOH	
	Dipole moment (e Å)	Polarizability (e^2 V^{-1})	Dipole moment (e Å)	Polarizability (e^2 V^{-1})
Fe-B_4	0.35	0.31	0.24	0.57
Fe-B_3C	0.38	0.25	0.17	0.53
Fe-B_3N	0.33	0.24	0.20	0.64
Fe-B_2C_2	0.32	0.25	0.09	0.57
Fe-B_2CN	0.30	0.25	0.20	0.55
Fe-B_2CO	0.31	0.20	0.08	0.45
Fe-B_2N_2	0.27	0.27	0.11	0.96
Fe-B_2NO	0.28	0.30	0.25	0.27
Fe-BCBC	0.32	0.29	0.01	0.14
Fe-BCCB	0.22	0.25	0.07	0.56
Fe-BC_3	0.27	0.30	-0.12	0.53
Fe-BC_2N	0.27	0.29	0.04	0.66
Fe-BC_2O	0.37	0.23	0.09	0.54
Fe-BCN_2	0.27	0.29	0.24	0.31
Fe-BNBN	0.49	0.27	0.41	0.53
Fe-BN_2B	0.41	0.31	0.08	0.63
Fe-BN_3	0.35	0.25	0.22	0.48
Fe-BN_2O	0.35	0.24	0.26	0.50
Fe-BNO_2	0.37	0.25	0.27	0.09
Fe-C_4	0.27	0.29	0.15	0.61
Fe-C_2NO	0.31	0.24	0.05	0.56
Fe-CN_2O	0.35	0.24	0.20	0.49
Fe-CNO_2	0.35	0.18	0.30	0.34
Fe-NC_3	0.35	0.27	0.12	0.63
Fe-N_2C_2	0.32	0.36	0.24	0.52
Fe-NCNC	0.33	0.22	0.18	0.35
Fe-N_2C_2	0.33	0.36	0.12	0.67
Fe-N_3C	0.32	0.25	-0.23	0.51
Fe-N_4	0.30	0.29	0.08	0.59
Fe-OB_3	0.37	0.26	0.22	0.65

Fe-OB_2O	0.54	0.22	0.39	0.58
Fe-OBOB	0.43	0.10	0.39	0.32
Fe-OC_3	0.37	0.33	0.06	0.51
Fe-OC_2O	0.47	0.22	0.29	0.47
Fe-OCOC	0.51	0.18	0.44	0.37
Fe-ON_3	0.33	0.22	0.32	0.33
Fe-ON_2O	0.37	0.14	0.31	0.23
Fe-ONON	0.38	0.17	0.33	0.33
Fe-O_2B_2	0.39	0.09	0.18	0.55
Fe-O_2C_2	0.34	0.21	0.00	0.59
Fe-O_3B	0.38	0.31	-0.01	0.78
Fe-O_3N	0.42	0.15	0.32	0.24
Co-O_3N	0.56	0.34	0.21	0.32
Ni-O_3N	0.55	0.43	0.02	0.92

Table S2

Table S2. Summary of the DFT-calculated energies, zero-point energies, heat capacities, and entropic contributions[7, 24]. Unit: eV.

Species	$\boldsymbol{E^{DFT}}$	***ZPE***	$\int C_p dT$	$-TS$
CO_2 (g)	-22.51	0.31	0.10	-0.66
H_2 (g)	-7.04	0.28	0.09	-0.40
CO(*g*)	-14.59	0.13	0.09	-0.61
*COOH	-	0.62	0.10	-0.19
*CO	-	0.19	0.08	-0.16

References

(1) Perdew, J. P.; Burke, K.; Ernzerhof, M. Generalized gradient approximation made simple. *Phys. Rev. Lett.* **1996**, *77* (18), 3865.

(2) Hammer, B.; Hansen, L. B.; Nørskov, J. K. Improved adsorption energetics within density-functional theory using revised Perdew-Burke-Ernzerhof functionals. *Phys. Rev. B* **1999**, *59* (11), 7413.

(3) Araujo, R. B.; Rodrigues, G. L. S.; dos Santos, E. C.; Pettersson, L. G. M. Adsorption energies on transition metal surfaces: towards an accurate and balanced description. *Nat. Commun.* **2022**, *13* (1), 6853.

(4) Wellendorff, J.; Silbaugh, T. L.; Garcia-Pintos, D.; Nørskov, J. K.; Bligaard, T.; Studt, F.; Campbell, C. T. A benchmark database for adsorption bond energies to transition metal surfaces and comparison to selected DFT functionals. *Surf. Sci.* **2015**, *640*, 36-44.

(5) Nørskov, J. K.; Rossmeisl, J.; Logadottir, A.; Lindqvist, L.; Kitchin, J. R.; Bligaard, T.; Jonsson, H. Origin of the overpotential for oxygen reduction at a fuel-cell cathode. *J. Phys. Chem. B* **2004**, *108* (46), 17886-17892.

(6) Ying, S. W.; Wang, Y.; Du, P.; Wang, Q.; Yue, C.; Zhang, D.; Chen, Z. C.; Zheng, J. W.; Xie, S. Y.; Li, H. C_{60} Fullerene as the Active Site for CO_2 Electroreduction. *Angew. Chem. Int. Ed.* **2025**, *64* (39), e202511924.

(7) Christensen, R.; Hansen, H. A.; Vegge, T. Identifying systematic DFT errors in catalytic reactions. *Catal. Sci. Technol.* **2015**, *5* (11), 4946-4949.

(8) Chen, L. D.; Urushihara, M.; Chan, K.; Nørskov, J. K. Electric Field Effects in Electrochemical CO2 Reduction. *ACS Catal.* **2016**, *6* (10), 7133-7139.

(9) Zhang, G.; Tan, B.; Mok, D. H.; Liu, H.; Ni, B.; Zhao, G.; Ye, K.; Huo, S.; Miao, X.; Liang, Z.; Liu, X.; Chen, L.; Zhang, Z.; Cai, W. B.; Back, S.; Jiang, K. Electrifying HCOOH synthesis from CO_2 building blocks over Cu-Bi nanorod arrays. *Proc. Natl. Acad. Sci.* **2024**, *121* (29), e2400898121.

(10) Li, H.; Kelly, S.; Guevarra, D.; Wang, Z.; Wang, Y.; Haber, J. A.; Anand, M.; Gunasooriya, G. T. K. K.; Abraham, C. S.; Vijay, S.; Gregoire, J. M.; Nørskov, J. K. Analysis of the limitations in the oxygen reduction activity of transition metal oxide surfaces. *Nat. Catal.* **2021**, *4* (6), 463-468.

(11) Li, H.; Long, J.; Jing, H.; Xiao, J. Steering from electrochemical denitrification to ammonia synthesis. *Nat. Commun.* **2023**, *14* (1), 112.

(12) Fumagalli, L.; Esfandiar, A.; Fabregas, R.; Hu, S.; Ares, P.; Janardanan, A.; Yang, Q.; Radha, B.; Taniguchi, T.; Watanabe, K.; Gomila, G.; Novoselov, K. S.; Geim, A. K. Anomalously low dielectric constant of confined water. *Science* **2018**, *360* (6395), 1339-1342.

(13) Kelly, S. R.; Kirk, C.; Chan, K.; Nørskov, J. K. Electric Field Effects in Oxygen Reduction Kinetics: Rationalizing pH Dependence at the Pt(111), Au(111), and Au(100) Electrodes. *J. Phys. Chem. C* **2020**, *124* (27), 14581-14591.

(14) Le, J.; Iannuzzi, M.; Cuesta, A.; Cheng, J. Determining potentials of zero charge of metal electrodes versus the standard hydrogen electrode from density-functional-theory-based molecular dynamics. *Phys. Rev. Lett.* **2017**, *119* (1), 016801.

(15) Duan, S.; Xu, X.; Tian, Z.-Q.; Luo, Y. Hybrid molecular dynamics and first-principles study on the work function of a Pt(111) electrode immersed in aqueous solution at room temperature. *Physical Review B* **2012**, *86* (4), 045450.

(16) Schnur, S.; Groß, A. Properties of metal–water interfaces studied from first principles. *New J. Phys.* **2009**, *11* (12), 125003.

(17) Sakong, S.; Groß, A. The electric double layer at metal-water interfaces revisited based on a charge polarization scheme. *J. Chem. Phys.* **2018**, *149* (8).

(18) Grimme, S.; Antony, J.; Ehrlich, S.; Krieg, H. A consistent and accurate ab initio parametrization of density functional dispersion correction (DFT-D) for the 94 elements H-Pu. *J. Chem. Phys.* **2010**, *132* (15), 154104.

(19) Heenen, H. H.; Gauthier, J. A.; Kristoffersen, H. H.; Ludwig, T.; Chan, K. Solvation at metal/water interfaces: An ab initio molecular dynamics benchmark of common computational approaches. *J. Chem. Phys.* **2020**, *152* (14).

(20) Sakong, S.; Forster-Tonigold, K.; Groß, A. The structure of water at a Pt (111) electrode and the potential of zero charge studied from first principles. *J. Chem. Phys.* **2016**, *144* (19).

(21) Trasatti, S. Structure of the metal/electrolyte solution interface: new data for theory. *Electrochim. Acta* **1991**, *36* (11), 1659-1667.

(22) Hansen, H. A.; Viswanathan, V.; Nørskov, J. K. Unifying Kinetic and Thermodynamic Analysis of 2 e^- and 4 e^- Reduction of Oxygen on Metal Surfaces. *J. Phys. Chem. C* **2014**, *118* (13), 6706-6718.

(23) Zhang, D.; Wang, Z.; Liu, F.; Yi, P.; Peng, L.; Chen, Y.; Wei, L.; Li, H. Unraveling the pH-Dependent Oxygen Reduction Performance on Single-Atom Catalysts: From Single- to Dual-Sabatier Optima. *J. Am. Chem. Soc.* **2024**, *146* (5), 3210-3219.

(24) Chan, K.; Tsai, C.; Hansen, H. A.; Nørskov, J. K. Molybdenum sulfides and selenides as possible electrocatalysts for CO_2 reduction. *ChemCatChem* **2014**, *6* (7), 1899-1905.